Excellent photo- and sono- catalytic BiOF/Bi_2O_3 heterojunction nanoflakes synthesized via pH-dependent and ionic liquid assisted solvothermal method

Zhuomin Qiang [a], Shiwen Zhu [a], Taohai Li [a, b], Feng Li [*a, b]

a. College of Chemistry, Key Lab of Environment Friendly Chemistry and Application in Ministry of Education, Xiangtan University, Xiangtan, 411105, China.

b. Nano and Molecular Materials Research Unit, Faculty of Science, University of Oulu, P.O. Box 3000, FIN-90014, Finland

[*]Corresponding author.

E-mail addresses: fengl_xtu@hotmail.com (F. Li)

Abstract: Herein, a series of BiOF/Bi_2O_3 heterojunction nanoflakes were designed. The XRD and TEM confirm that the phase structure and morphology of BiOF/Bi_2O_3 were affected by the pH value of the precursors. The catalytic activities were investigated in different catalytic ways including photocatalytic activity under ultraviolet light, photocatalytic activity under visible light and sonocatalytic activity under ultrasonic irradiation. It concluded that the catalytic performances of BiOF/Bi_2O_3 are substantially affected by laboratorial pH values. The BiOF/Bi_2O_3 prepared at lower pH values exhibited enhanced catalytic activity attributed to the favorable morphology and band gap energy. Meanwhile, it shows excellent sonocatalytic performances due to the synergistic effect of BiOF/Bi_2O_3 and H_2O_2 in sonocatalytic process. The sonodegradation efficiencies of rhodamine B reaches 95.28 % in the presence of three drops of H_2O_2 within 10 minutes of ultrasonic irradiation. The catalytic mechanism reveals that ·OH as the dominant active specie plays a key role in degrading the dyes both under UV light illumination and ultrasonic irradiation.

Keywords: Solvothermal method; BiOF/Bi_2O_3; Photocatalytic; Sonocatalytic

1. Introduction

Bismuth oxyhalide, the BiOX, refers to a group of ternary oxide semiconductors, where X is the halogen element such as F, Cl, Br, and I. Due to unique layered structure, photogenerated e^--h^+ pairs are prompted on these semiconductor catalysts, resulting in high photocatalytic activities [1-3]. Yet study of this group of photocatalysts has become one of the research focuses within today's catalysis. In a latest study, we have shown that the presence of BiOCl synthesized possessed excellent photocatalytic activities, which greatly accelerated to the photodegradation of organic dyes with the illumination of visible light and sunlight [4]. Similarly, Huo et al have previously reported the synthesis of hierarchical BiOBr microspheres which exhibited high photoactivities for degrading rhodamine B (RhB) under visible radiation [5]. Synthesized via a one-step solution method, the as-prepared mesoporous BiOI microspheres were found to have removal ability to tetracycline hydrochloride (TC) under visible light irradiation [6]. Despite of many progresses to develop BiOX (X = Cl, Br, I) semiconductors, however, there are much less studies on BiOF semiconductors. To the best of our knowledge, a few prior works have been carried out for synthesis and functionalities of the BiOF photocatalysts [7-9]. These works, either suffer from stringent reaction conditions with calcination temperature at 400 °C, as well as using Azadirachta indica leaf extract and its flavonoid constituent i.e. quercetin during preparation of pure tetragonal BiOF, or lack of more general catalytic functionalities e.g. photocatalysis under the visible light radiation or other energy sources. Additionally, impact from synthesis parameters such as the pH values has not been well explored for the bismuth oxyhaide growth and the binary composites of BiOF/Bi_2O_3 with heterogeneous structure were rarely reported.

It is well-known that photocatalytic abilities can be enhanced in properly designed semiconductor heterojunctions where photoinduced charges (either e^- or h^+) can migrate crossing the interface, reducing the recombination probability of the e^--h^+ pairs. Due to this reason, the BiOX has also been

engineered into the heterojunction forms. For instance, heterojunctional BiOCl/BiOI [10] and $BiOCl/Bi_2O_3$ [11] possess better visible light catalytic abilities than their monocomposite photocatalyst, the BiOCl. Such a trend has also been revealed in the $BiOCl/(BiO)_2CO_3/Bi_2O_3$ ternary photocatalyst in microflower forms [12]. Despite of these progresses, however, reports on BiOF heterojunction forms have never been seen to the best of our knowledge. This may partially due to the stringent preparation routes which limits the formation of BiOF when contact other composites.

Among various ambiences during the catalyst synthesis, ionic liquids (ILs), have gained a great deal of attention as a neoteric kind of reaction media [13] in inorganic nanomaterials preparation in virtue of these unique superiorities, such as extremely high thermal stability, good dissolving ability, low volatility, negligible vapor pressure, low melting point and designable structures [14,15]. Taking the above advantages of ionic liquids into account, the BiOF heterojunctions may be formed once proper ionic liquids are employed as reaction reagents.

Energy supplies in the indispensable catalytic reactions are not limited to the form of light. Similar to photon, phonon also represents another kind of energy carrier. Correspondingly, sonocatalysis is also a promising technology for ultrasonic degradation of organic pollutants besides the photocatalysis technique [16-20]. Reaction in sonocatalysis can be formed in the following stages. Firstly, the light with a relatively wide wavelength range can be formed of the ultrasonic radiation, which can motivate the semiconductor that acts as a photocatalyst to generate e^--h^+ pairs [21]. Secondly, the reactive species including ·OH, ·OOH from H_2O molecules are manufactured via transitory collapse of cavitation bubbles actuated by ultrasound radiation during the reaction, meanwhile the acoustic cavitation can fabricate numerous hot spots possessed regionally high temperatures and pressures in a brief period [20]. The sonocatalystic reaction scheme is very similar to the photocatalytic ones where photogenerated electrons and holes may react with O_2 or H_2O to

form $\cdot O_2^-$ and ·OH [22-24]. Therefore, using ultrasonic as the primary source may also lead to degradation of organic dyes with the existence of synthetic BiOX heterojunctions.

In this work, we report on the first realization of excellent photo- and sono- catalytic BiOF/Bi_2O_3 heterojunction nanoflakes synthesized via a facile ionic liquid assisted one-pot solvothermal method. The effect of the pH values with wide range (from 1 to 11) on the properties (phase composition, morphology and catalytic performances) of BiOF/Bi_2O_3 catalysts was systematically investigated. Moreover, the catalytic performance of the obtained BiOF/Bi_2O_3 nanoflakes was evaluated not only under light irradiation but also under ultrasonic irradiation. This work shows potentials of using BiOF/Bi_2O_3/other semiconductor catalysts for water treatments in addition to the facile routes to synthesize photocatalysts of similar type.

2. Experimental

2.1 Preparation of BiOF/Bi_2O_3 catalyst

All the chemical were used as received without further purification. In a traditional synthesis, $Bi(NO_3)_3 \cdot 5H_2O$ (1.213 g) and the ionic liquids $[BMIM]BF_4$ (0.424 g) were respectively added into 8 mL of ethanol under continuously agitation for 20 min. The mixture was obtained by adding $[BMIM]BF_4$ solution to the $Bi(NO_3)_3$ solution dropwise, while stirring at room temperature for 20 min, and the pH was kept in a fixed value through HF/$NH_3 \cdot H_2O$ solution. Then, the suspensions were kept for 24 h at 160 ^oC in Teflon-lined stainless steel autoclave with a capacity of 25 mL. Finally, the samples were prepared after washed and dried at 70 ^oC for 12 h. The samples were labeled as SX (X represents the pH values adjusted in the synthesis process).

2.2 Characterizations

The crystalline phase of the samples was analyzed by X-ray diffraction (XRD, MiniFlex II) using diffractometer with Cu Kα radiation (λ = 0.15406 nm). Scanning Electron Microscopy (SEM, JEOLJSM-6700F) and transmission electron microscope (TEM, JEM-2010) were employed to research the morphology of the prepared samples. The elements on the surface of the sample were investigated by X-ray photoelectron spectroscopy (XPS, pHI 5300), which was carried out using a monochromatic Mg Kα source. The UV-vis diffuse reflectance spectra (DRS, Lambda-25) were recorded over the spectral range 200-800 nm. The photoluminescence (PL) emission spectra of as-obtain samples was documented on a flurescence spectrometer (PL, LS55) at room temperature with excitation wavelength 270 nm. The electrochemical impedance spectroscopy (Mott-Schottky plots) was performed on an electrochemical workstation (CHI660E) in a typical three-electrode system.

2.3 Photocatalytic activity measurement

The contaminant removal ability of the samples prepared were assessed by using rhodamine B (RhB) molecules as typical pollutants in water under ultraviolet light (using a 500 W mercury lamp) and visible radiation (using a 350W Xe lamp equipped with a 400 nm cut-off filter), respectively. All the photocatalytic experiments were executed at room temperature as follows: 50 mg catalysts were decentralized in 50 mL RhB aqueous solution (10 mg L^{-1}) under constant magnetic stirring. Before the lighting radiation, the suspension was stirred by magnetic force under darkness for 30 min to achieve an adsorption-desorption equilibrium between the dyestuff molecules and photocatalysts. Afterwards, the light source was turned on. Within a given time interval, 5 mL of the suspension was collected and the precipitates were eliminated by centrifugation (3500 rpm, 5 min). The concentration of RhB was supervised through checking the absorption spectrum of each sample.

2.4 Sonocatalytic activity measurement

Sonocatalytic degradation activities of RhB were also studied in the existence of the $BiOF/Bi_2O_3$ synthesized catalyst by ultrasonic reactor with an ultrasonic frequency of 40 kHz and output power of 200 W. In a typical process, 50 mg catalyst, three drops of H_2O_2 and 10 mg L^{-1} RhB concentration in 50 mL total volume were adopted to perform the sonocatalytic degradation. Prior to the ultrasonic irradiation, the gained suspension was continually agitated for 30 min in the dark to achieve the absorption-desorption equilibrium of the RhB and catalyst. In order to avoid photoexcitation of the $BiOF/Bi_2O_3$ particles, the sonocatalytic reactions were executed under the dark environment. Within the specified time intervals, 3 mL of the ultrasonicated suspension was taken out and centrifuged to detach the precipitation, then the absorbance of the solution was recorded by a UV-vis spectrophotometer at 554 nm of fixed absorption wavelength of RhB.

2.5 Reactive species analysis

In order to evaluate the types of possible reactive species participated in the photocatalytic and sonocatalytic reaction, the various quenchers were selected to capture the relevant reaction species, which is analogue to the photocatalytic degradation process. Three scavengers, benzoquinone (BQ, 2 mmol L^{-1}), isopropanol (IPA, 10 mmol L^{-1}) and disodium ethylenediaminetetraacetate (EDTA-2Na, 5 mmol L^{-1}) were added in the aqueous solution of RhB (10 mg L^{-1}) before the addition of the photocatalyst to trap the active species.

3. Results and Discussion

3.1 Structural characterization

The XRD patterns of the catalysts fabricated at various pH values were revealed in Fig. 1. It can be clearly observed that initial pH value of precursors significantly impacts the structural properties of the obtained products. Fig. S1 (SI) specifically shows the XRD patterns of the samples. In Fig.

S1a, the sample prepared at pH = 1 with lattice constants a = 0.5853 Å, b = 0.5853 Å and c = 0.5853 Å was indexed to BiF_3 of cubic phase (the space group P-43m) with the JCPDS file NO. 65-9744. As the pH was adjusted to 2-4, (Fig. S1b), the sharp and narrow peaks indicate that the samples, which are indexed to tetragonal BiOF with the space group P4/nmm, are well crystallized. Besides, the peak at 27.25^o is attributed to (111) crystal phase of cubic Bi_2O_3 with the space group Fm-3m (JCPDS NO. 16-0654). Moreover, a weak peak at 26.359^o is also observed when the pH was turned to 4, which was indexed to the cubic phase of BiF_3. The results suggest that the sample is composed of tetragonal BiOF and cubic Bi_2O_3 when the pH value was turned to 2-4. The XRD patterns of the products prepared at pH = 5-6 (Fig. S1c) indicate the coexistence of tetragonal BiOF (JCPDS NO. 22-0114) and cubic BiF_3 (JCPDS NO. 65-9744). As the pH value increased to 9-11 (shown in Fig. S1d), the samples are in conformity to tetragonal BiOF and cubic Bi_2O_3. Interestingly, it is found that with the pH value increasing from 7 to 11, the intensity of the (111) peak at 27.25^o (cubic Bi_2O_3) was enhanced while the intensity of the (002) peak at 28.68^o (tetragonal BiOF) was decreased. From the above results, BiOF/Bi_2O_3 composites can be obtained when the pH value was adjusted to 2-4 and 7-11. Besides, the growth of (002) crystal plane of tetragonal BiOF at 28.68^o can be controlled only by turning the pH value from 7-11.

Fig. 1

3.2 Morphological characterization

The surface morphology and microstructural features of the as-obtained BiOF/Bi_2O_3 were confirmed by SEM images which are shown in Fig. 2 (also seen in Fig. S2). As can be seen in Fig. 2a (Fig. S2a), the BiF_3 (S1) is composed of the blocky particles with the size of about 3-5 μm. In Fig. 2b-e (Fig. S2b-e), the BiOF/Bi_2O_3 prepared at acidic conditions (pH = 2-4) is consist of large numbers of uniform nanoflakes with the diameters of 0.8-1 μm. Interestingly the nanoflakes seem to agglomerate to microflowers when the pH value increased to 4 (Fig. 2d, S2d), which is probably

ascribed to the appearance of the cubic BiF_3 as denoted by the weak peak at 26.359^o in Fig. S1b. For the samples fabricated at pH = 5-6, the BiOF/BiF_3 samples (Fig. 2e-f, S2e-f) show the tendency of microsphere structure self-assembled by the nanoflakes which surface are coated by many nanoparticles. The BiOF/Bi_2O_3 prepared at basic conditions (pH = 7-11) is shown in Fig. 2g-i (Fig. S2g-i), it can be found that the sample with sheet-like shapes and the diameters is around 0.6-3 µm. It is worth noting that the particles are getting thicker along with the increasement of pH from 7 to 11 due to the growth of (111) crystal phase of cubic Bi_2O_3. It is noticeable, meanwhile, that the BiOF/Bi_2O_3 fabricated in basic conditions is thicker than those prepared in acidic conditions.

Fig. 2

The representative TEM images of the prepared BiOF/Bi_2O_3 (S2) are shown in Fig. 3, where the detailed morphological information of the prepared samples can be obtained. As displayed in Fig. 3a-c, BiOF/Bi_2O_3 has a lamellar morphology, which match well with the results of SEM. The corresponding HRTEM image in Fig. 3d showing lattice fringes corresponding to the interplanar distance of 0.333 nm is ascribed to the (111) plane of cubic Bi_2O_3. Meanwhile, another lattice spacing of 0.313 nm is in accordance with the (002) crystal plane of the tetragonal BiOF. Moreover, the boundary between BiOF and Bi_2O_3 and obvious lattice fringes can be clearly observed in Fig. 3, suggesting the formation of heterojunctions materials with excellent crystallinity, which can benefit better charge separation and transfer within the hybrid structure.

Fig. 3

3.3 XPS exploration

Additionally, XPS measurement was carried out to investigate the elemental composition and chemical states of the as-prepared BiOF/Bi_2O_3 (S2) powder. Fig. 4a shows the overall XPS spectra of pure BiOF/Bi_2O_3 prepared at pH = 2 (S2) composite catalysts. A general survey in Fig. 4 verifies

that obtained S2 sample consists of the elements Bi, O, F. The high resolution XPS spectra of S2 samples are shown in Fig. 4b-d. Peak of C is attributed to the extraneous hydrocarbon owing to the XPS test instrument itself. In Fig. 4b, the binding energies at 159 and 164.68 eV are from Bi $4f_{7/2}$ and Bi $4f_{5/2}$ of Bi^{3+}, respectively [17,25-26]. In the spectrum of O 1s, the peak with binding energy of 530.18 eV (Fig. 4c) is associated with the Bi-O bonds corresponded to the $(Bi_2O_2)^{2+}$ sheets of BiOX stratified structure [27]. The peaks with 683.2 eV in the spectrum of F 1s suggest the presence of BiOF [28]. The XPS analysis proves that the as-synthesized sample (S2) is the composite of BiOF and Bi_2O_3, which are in great consistent with those results for XRD.

Fig. 4

3.4 Optical properties

The energy band structure character of semiconductor materials is identified as a critical factor to confirm their photocatalytic activity and sonocatalytic activity. Thus, we measured the optical absorption property and the band gap energy of the prepared BiOF/Bi_2O_3 samples utilizing a UV-vis spectrophotometer, the results are shown in Fig. 5. S2 has the highest absorption in UV light range with the wavelength of 200-400 nm, followed by S11, S3, S9 and S4. And BiOF/Bi_2O_3 prepared at pH = 7 exhibits the lowest absorption in the range of ultraviolet wavelengths. As for the optical absorption property within the range of visible wavelengths, it can be seen that sample S7, S9 and S11 have nearly no absorption in the wavelength range of 400-800 nm while sample S2, S3 and S4 have little absorptions. Besides the optical absorption property, the band gap energy is another important information which can be obtained in UV-vis DRS. Fig. 5 suggests that the absorption edge of the obtained sample S2, S3, S4, S7, S9 and S11 are found at 325.8 nm, 310.1 nm, 311.6 nm, 320.6 nm, 311.4 nm and 310.8 nm, respectively. Their corresponding band gap energy (E_g value) are 3.806 eV (S2), 3.999 eV (S3), 3.979 eV (S4), 3.868 eV (S7), 3.982 eV (S9) and 3.990 eV (S11), respectively. Therefore, the UV-vis absorption results prove that S2 can obtain strongest absorption

in UV light region and has the narrowest band gap energy (3.806 eV). The E_g value of S2 is a little narrower than pure BiOF (3.95 eV) as reported in the literature, which is ascribed to the formation of BiOF/Bi_2O_3 heterojunction contributed to adjust the relative position of their energy bands [7].These results indicated that the BiOF/Bi_2O_3 composite with heterogeneous structure have huge potential to remove organic pollutants under illumination and ultrasonic irradiation.

Fig. 5

In addition, it is known that the band edge position of the BiOF and Bi_2O_3 directly decide the interface migration pathways of the charge carriers. In order to investigate the effect of band structure of the BiOF/Bi_2O_3 composite (S2), the potentials of valence band (VB) of BiOF and Bi_2O_3 are calculated by Mulliken electronegativity theory: $E_{VB} = X - E^e + 0.5E_g$, where X is defined as the electronegativity of the semiconductor, E^e is the energy of the free electrons on the hydrogen scale (ca. 4.5 eV), E_g is the band gap energy of the semiconductor. The potentials of conduction band (CB) edges can be calculated by $E_{CB} = E_{VB} - E_g$ [29]. The results were shown in Table S1. For BiOF, the E_{VB} and E_{CB} are estimated to 4.50 eV and 0.54 eV, respectively. Therefore, according to the above equations, the E_{VB} and the E_{CB} of Bi_2O_3 are calculated to 2.54 eV and 0.19 eV, respectively. From the above results the possible charge transfer process over BiOF/Bi_2O_3 under UV illumination and ultrasonic irradiation is proposed in the following section.

In order to understand the enhanced photocatalytic activity of the BiOF/Bi_2O_3 samples, the photoluminescence (PL) spectra with excitation wavelength of 270 nm are obtained. In PL spectra, higher intensity can be ascribed to the high rate of electron-hole recombination. As can be seen in Fig. 5c-d, BiOF/Bi_2O_3 exhibits a strong emission band at approximately 408 nm, which is derived from the band-gap recombination of e^--h^+ pairs. Apparently, the PL intensity of S2 is much lower than other samples. Thus, the recombination of photoinduced carriers in BiOF/Bi_2O_3 would be significantly suppressed, which may be due to the formation of heterojunction.

3.5 Photocatalytic activity under UV light irradiation

The ultraviolet light photocatalytic degradation of RhB in sewage was chose as a model to research the photocatalytic performances of BiOF/Bi_2O_3 composites. Fig. S3 presents the variations of RhB concentration over different samples. From Fig. S3a-c, it can be clearly seen that S2 and S3 samples reveal the more excellent photocatalytic property relative to S4. The photocatalytic activity of BiOF/Bi_2O_3 prepared under basic conditions (pH = 7-11) was shown in Fig. S3d-f. Interestingly, S7 showed the highest photocatalytic performance for degradation of RhB, followed by S9, and S11 has the lowest photocatalytic activity. Thus, as for BiOF/Bi_2O_3 prepared at pH = 7-11, a higher pH value of the synthesis solution leads to lower photocatalytic activity of the as-prepared catalysts. Besides BiOF/Bi_2O_3 catalysts, the photocatalytic performances of pure BiF_3 (S1) and BiOF/BiF_3 (S5) were also investigated. The results are depicted in Fig. S3g-h. The as-synthesized Bi_2O_3 can completely degrade RhB after UV light irradiation within 140 min (Fig. S3g) and the BiOF/BiF_3 (S5) catalysts can degrade all of RhB dyes after 100 min. These results indicate that S2, S3, S7 shows high photocatalytic activity by degrading RhB under UV light.

Fig. 6 shows the photocatalytic degradation curves of RhB as a function of time. As shown in Fig. 6a, after 20 min of UV light irradiation, the photocatalytic activities of diverse photocatalysts comply the order of S4 < S3 < S2, which efficiencies of RhB are 18.25 %, 99.05 % and 100 %, respectively. It is distinctly seen that the concentration of RhB alters mildly with the identical reaction conditions (the photolysis test) without photocatalyst for comparison, indicating that the self-photolysis of dye is extremely astricted and can be insignificant. Thus, under UV light irradiation, S2 and S3 exhibit the exceedingly good photocatalytic activity, which are approximately 5.4 and 5.5 times compared with S4, respectively. This is probably ascribed to the appearance of the peak indexed to Bi_2O_3 at 26.359^o. Besides, the slight agglomeration of nanoflakes (seen in Fig. 2d and Fig. S2d) may lead to poor photocatalytic activity of S4.

However, the trend of photocatalytic ability is different for $BiOF/Bi_2O_3$ prepared at basic conditions. It is observed from Fig. 6b that S7 can completely degrade RhB after UV light illumination for 40min. Moreover, the photodegradation efficiencies of RhB can reach as 97.52 % and 57 % for S9 and S11, respectively within 100 min. It can be concluded that the photocatalytic performance for the obtained $BiOF/Bi_2O_3$ samples (prepared at pH = 7-11) is higher when the pH value of the synthesis precursor is lower. Furthermore, the photocatalytic performance of S2 is more splendid than S11, which is possibly attributed to the thicker nanoplates covering the active sites of S11 and impeding the light absorption, leading to low photodegradation efficiency.

Fig. 6

3.6 Photocatalytic activity under visible light irradiation

In addition to photo- and sono- catalytic activity, the adsorbability for RhB of photocatalysts is another important issue for their practical applications, therefore, we studied the adsorption-desorption experiments of $BiOF/Bi_2O_3$ in the dark conditions. In Fig. 6-8, the adsorption efficiency for RhB of $BiOF/Bi_2O_3$ prepared at pH =2, 3, 4, 7, 9, 11 was obtained through adsorption dye for 30 min in darkness, which ensure the adsorption/desorption equilibrium before irradiation and ultrasound. Moreover, Fig. S4 shows the adsorption and desorption rates of RhB dye over different samples. We can see that adsorption performance of all samples remains stable after 30 min and S2 exhibited higher adsorption activity other composites (Fig. S4a), which attributed to different specific surface area and pore size distribution. Desorption studies indicate that all of samples exhibit higher elution efficiency as shown in Fig. S4b. According to the results, the tests presented low adsorption efficiency of RhB and high desorption efficiency in darkness, indicating that we could neglect the adsorption effect of photocatalysts.

The photocatalytic activity of $BiOF/Bi_2O_3$ beneath visible light was evaluated by degrading RhB. After irradiation of 120 min, nearly 100 % (S2), 86.99 % (S3), 40.84 % (S4), 52.45 % (S7), 25.67 %

(S9) and 19.87 % (S11) of RhB were removed in the presence of three drops of H_2O_2 (Fig. 7a). Fig. 7b shows photocatalytic results of the obtained BiOF/Bi_2O_3 photocatalysts for RhB without adding H_2O_2 scavenger. From Fig. 7b, all of the samples have poor photoactivity for degrading RhB under visible light irradiation. This is probably owing to the poor adsorptive property and tough migration of electron-hole pairs. In addition, about 2 % RhB was degraded when only three drops of H_2O_2 were added in the photolysis test. Thus, the RhB can only be degraded in the existence of BiOF/Bi_2O_3 and H_2O_2. This is because the photogenerated electrons can cooperate with H_2O_2 to form more •OH, which is beneficial to separate electron-hole pairs and generate more reactive species •OH.

Fig. 7

3.7 Sonocatalytic activity

To compare the effect of different catalytic ways, we also degrade RhB under ultrasonic irradiation. The sonocatalytic degradation curves and the relevant variations of UV-vis spectra of RhB with prolongation react time are displayed in Fig. S5. From Fig. S5a, in the presence of three drops of H_2O_2, S2 can degrade the most of RhB after ultrasonic irradiation during an extremely short time of 10 min. Besides, S2 showed the highest sonocatalytic performance for degrading of RhB, followed by S3, and S4 has the lowest sonocatalytic activity (Fig. S5b-c). It seems that BiOF/Bi_2O_3 prepared at lower pH values has more excellent sonocatalytic activity. This may be ascribed to the morphology and band gap energy. Thinner nanoflakes and narrower band gap may be beneficial to the sonocatalytic performance of the semiconductors. Fig. S5d-f presents the sonocatalytic activity of BiOF/Bi_2O_3 prepared under basic conditions. Similarly, BiOF/Bi_2O_3 prepared at higher pH values (S11) has the lowest sonocatalytic activity.

The sonocatalytic disintegration of RhB was assessed to investigate the catalytic activity of as-synthesized samples (Fig. 8) in the presence of three drops of H_2O_2. In Fig. 8a, the sonodegradation efficiencies of RhB are 97.95 %, 96.85 %, 95.44 %, 89.93 %, 77.24 % and 36.79 % for S2, S3, S4,

S7, S9 and S11, respectively within 60 min of ultrasonic irradiation. This suggests that $BiOF/Bi_2O_3$ prepared at lower pH values can degrade RhB more effectively in the presence of three drops of H_2O_2. In comparison, the stability of RhB was similarly authenticated without any catalysts in the selfsame circumstance (blank experiment), which suggests that the efficiency of ultrasonic irradiation alone on the self-sonolysis of RhB was inefficient.

In order to illustrate the synergistic effect of $BiOF/Bi_2O_3$ and H_2O_2 in sonocatalytic process, the sonodegradation of RhB without adding H_2O_2 or only adding three drops of H_2O_2 was conducted under the same conditions. As shown in Fig. 8b, when H_2O_2 was not added in sonocatalytic process, ultrasonic irradiation in 60 min induces a bit low removal rate of RhB for $BiOF/Bi_2O_3$ samples. And in the same time, the sonodegradation rate of RhB in the presence of only three drops of H_2O_2 is 24.29 %. These results demonstrate rather low synergistic effect of $BiOF/Bi_2O_3$ and H_2O_2 in sonocatalytic process. It can be concluded from the above results that $BiOF/Bi_2O_3$ fabricated at pH = 2 exhibits the best sonocatalytic activity.

Fig. 8

3.8 Photocatalytic and sonocatalytic mechanisms

To evaluate the role of reactive species in catalytic process, various scavengers were introduced to the degradation system. The trapping experiments were accomplished with the presence of $BiOF/Bi_2O_3$ (S2) catalyst using benzoquinone (BQ) as the $\bullet O_2^-$ scavenger, disodium ethylenediaminetetraacetate (EDTA-2Na) as the h^+ scavenger and isopropanol (IPA) as the •OH scavenger, respectively.

The UV light source was selected for the radical trapping tests due to the unification of photocatalytic mechanism under visible and ultraviolet light. Fig. 9a shows the photocatalytic activity of $BiOF/Bi_2O_3$ (S2) toward the remove of RhB after injecting the radical scavengers. When 1mM IPA was introduced into the degradation system, the decrease in the photocatalytic oxidation

efficiency of RhB over S2 is the most obvious, meaning •OH plays a vital part in the degradation reaction. The addition of BQ and EDTA-2Na led to segmental restraint for the degradation of RhB, suggesting that $•O_2^-$ and h^+ played a minor function in the photocatalytic quenching experiments. For further confirmation of active role of •OH, terephthalic acid (TA) is diffusely employed as employed search [30]. As shown in Fig. 9c, the confirmatory test of •OH by using TA as a survey reagent is exhibited, and it does not react with other radicals. In fluorescence spectra analysis, the solution showed a peak at λ = 426 nm under excitation at λ = 315 nm, which confirms the formation of 2-hydroxyterephthalic acid (HTA). According to the discussions, it can be inferred that the photocatalytic oxidation remove of RhB was actuated principally through the generation of •OH radicals and the $•O_2^-$ played a secondary role and holes to a lesser extent participated in that process.

Fig. 9

In addition, it is essential to investigate the possible reaction mechanism in order to preferably master the enhancement of RhB degradation under UV light irradiation. As stated above, The CB values of BiOF and Bi_2O_3 are 0.54 and 0.19 eV, respectively and their VB values are 4.50 and 2.54 eV, respectively. Besides, from the Mott-Schottky plot of BiOF/Bi_2O_3 (S2) shown in Fig. S6, it is confirmed that the heterojunction material was composed of p-type semiconductor of BiOF and Bi_2O_3 [31]. As illustrated in Scheme 1a, the energy of UV light excites BiOF and Bi_2O_3 to produce photogenerated e^--h^+ pairs. Afterwards, the photogenerated electrons in the Bi_2O_3 conduction band (CB) may transfer to the CB of BiOF, to further react with O_2 and generate the reactive radicals ($•O_2^-$). Meanwhile the residual h^+ in the BiOF valence band (VB) may transfer to the VB of Bi_2O_3, resulting in the generation of radicals •OH (the major active species responsible for the photodegradation reaction). These reactive radicals (•OH, $•O_2^-$) can degrade RhB to CO_2 and H_2O. Thus it can be seen the conception of BiOF/Bi_2O_3 heterojunction facilitates effectually the separation of photon-generated carriers to enhance tremendously photocatalytic ability.

We also studied the sonocatalytic reaction scheme by introducing various scavengers to the sonocatalysis. As shown in Fig. 9b, the sonocatalytic degradation efficiency was extremely suppressed with the addition of IPA while negligibly affected by BQ and EDTA-2Na, which manifests main roles of •OH and the less impact of $•O_2^-$ and h^+ in the sonocatalytic degradation reaction. In addition, the PL spectral observation from sonocatalysis of TA is plotted in Fig. 9c. High fluorescent intensity confirms the adequate generation of •OH [32].

Basis upon the above conclusions and the demonstration of CB and VB positions, a possible sonocatalytic degradation mechanism was proposed. As depicted in Scheme 1b, the light hot energies (sonoluminescence) resulted from the cavitation of ultrasonic irradiation can excite the Bi_2O_3 catalysts to generate e^--h^+ pairs. The sono-generated electrons (e^-) can transfer from CB of Bi_2O_3 to CB of BiOF due to the more positive CB potential of BiOF compared to Bi_2O_3, and the electrons were trapped by H_2O_2 to form •OH radicals to disintegrate organic dyes, which suggests the formation of BiOF/Bi_2O_3 heterojunction inhibited the recombination of e^--h^+ in the composite [33]. Simultaneously, the holes in the valence band (VB) of Bi_2O_3 reacted with H_2O/OH^- to form •OH reactive species. These highly active radicals exhibit remarkable oxidizing ability to the dyes (RhB).

Catalytic mechanisms show similarity and differences in photo- and sono- catalysis. In both cases, •OH play important roles, following the electrons migrations from the Bi_2O_3 to the bismuth oxyhalide site. Differences mainly arise from the migration of the positive charges of h^+. While h^+ migrates from BiOF to the oxide site in photocatalysis (Scheme 1a), it is only produced and trapped in the energetically lower valance band at the Bi_2O_3 side during sonocatalysis (Scheme 1b). Indeed, such a charge migration also bears the combined influences of the bandgap and source energy. The UV light typically has higher energy than the photons produced in cavitation [34]. This allows the

photoexcition of electrons from VBs to the CBs in BiOF with even higher bandgap than the Bi_2O_3. The holes of BiOF will migrate to the energetically lower VB of Bi_2O_3. On the opposite, sonoenergy is just enough to create e^--h^+ pair at Bi_2O_3 of narrower bandgap but not in the BiOF site. While the e^- can migrate to the higher energy site of floride, the sonoinduced h^+ remains at the energetically lower basin at the oxide site.

Scheme 1

4. Conclusions

In conclusion, the BiOF/Bi_2O_3 heterojunction was synthesized through a simple one-step method of the ionic-liquid cooperated solvothermal method. The experimental results indicate that pH has a significant effect on the morphology and catalytic activity of BiOF/Bi_2O_3. When prepared at lower pH values (pH = 2), the BiOF/Bi_2O_3 composed by relatively thin nanosheets exhibits optimal catalytic activity on the degradation of RhB under light or ultrasonic irradiation. Through the detection of reactive species, it is found that ·OH was the foremost active species in degrading the dyes both under UV light illumination and ultrasonic irradiation. Therefore, the BiOF/Bi_2O_3 catalyst may improve the photocatalytic activity of environmental application.

Acknowledgements

The authors acknowledge with thanks the financial support of Hunan 2011 Collaborative Innovation Center of Chemical Engineering & Technology with Environmental Benignity and Effective Resource Utilization and the National Natural Science Foundation of China (21343008; 21601149). Feng Li thanks the support of China Scholarship Council.

Conflict of interest

The authors declare no conflict of interest.

Reference

[1] H.F. Cheng, B.B. Huang, Y. Dai, Engineering BiOX (X= Cl, Br, I) nanostructures for highly efficient photocatalytic applications, Nanoscale 6 (2014) 2009-2026.

[2] K.H. Reddy, S. Martha, K.M. Parida, Fabrication of novel p-BiOI/n-ZnTiO3 heterojunction for degradation of rhodamine 6G under visible light irradiation, Inorg. Chem. 52 (2013) 6390-6401.

[3] Z.M. Qiang, J.Q. Huang, C.Y. Yang, F. Li, T.H. Li, M. Huttula, Z. J. Huang, W. Cao, A facile synthesis of heterojunctional $BiVO_4/Bi_5O_7I$ with enhanced photocatalytic activity for organic dyes degradation, J. Inorg. Organomet. P. (2019) 1-10.

[4] C.Y. Yang, F. Li, T.H. Li, W. Cao, Preparation and first-principles study for electronic structures of BiOI/BiOCl composites with highly improved photocatalytic and adsorption performances, J. Mol. Catal. A 418 (2016) 132-137.

[5] Y.N. Huo, J. Zhang, M. Miao, Y. Jin, Solvothermal synthesis of flower-like BiOBr microspheres with highly visible-light photocatalytic performances, Appl. Catal. B 111 (2012) 334-341.

[6] R. Hao, X. Xiao, X.X. Zuo, J.M. Nan, W.D. Zhang, Efficient adsorption and visible-light photocatalytic degradation of tetracycline hydrochloride using mesoporous BiOI microspheres, J. Hazard. Mater. 209 (2012) 137-145.

[7] W.Y. Su, J. Wang, Y.X. Huang, W.J. Wang, L. Wu, X.X. Wang, P. Liu, Synthesis and catalytic performances of a novel photocatalyst BiOF, Scrip. Mat. 62 (2010) 345-348.

[8] S.J. Zou, F. Teng, C. Chang, Z.L. Liu, S.R. Wang, Controllable synthesis of uniform BiOF nanosheets and their improved photocatalytic activity by an exposed high-energy (002) facet and internal electric field, RSC Adv. 5 (2015) 88936-88942.

[9] M. Yadav, S. Garg, A. Chandra, K. Hernadi, Quercetin-sensitized BiOF nanostructures: An investigation on photoinduced charge transfer and regeneration process for degradation of organic pollutants, J. Photoch. Photobio. A. 383 (2019) 112014.

[10] C.Y. Yang, F. Li, M, Zhang, T.H. Li, W, Cao, Preparation and first-principles study for electronic structures of BiOI/BiOCl composites with highly improved photocatalytic and adsorption performances, J. Mol. Cat. 426 (2016) 1-11.

[11] S.Y. Chai, Y.J. Kim, M.H. Jung, A.K. Chakraborty, D. Jung, W.I. Lee, Heterojunctioned BiOCl/Bi_2O_3, a new visible light photocatalyst, J. Catal. 262 (2009) 144-149.

[12] A. Etogo, E. Hu, C.M. Zhou, Y.J. Zhong, Z.L. Hong, Facile fabrication of mesoporous BiOCl/$(BiO)_2CO_3$/Bi_2O_3 ternary flower-like heterostructured microspheres with high visible-light-driven photoactivity, J. Mater. Chem. A 3 (2015) 22413-22420.

[13] W.J. Zheng, X.D. Liu, Z.Y. Yan, L.J. Zhu, Ionic liquid-assisted synthesis of large-scale TiO_2 nanoparticles with controllable phase by hydrolysis of $TiCl_4$, ACS Nano. 3 (2009) 115-122.

[14] J.B. Lian, X.C. Duan, J.M. Ma, P. Peng, T. Kim, W.J. Zheng, Hematite (α-Fe_2O_3) with various morphologies: Ionic liquid-assisted synthesis, formation mechanism, and properties, ACS Nano. 3 (2009) 3749-3761.

[15] H. Choi, Y.J. Kim, R.S. Varma, D.D. Dionysiou, Thermally stable nanocrystalline TiO_2 photocatalysts synthesizedvia sol-gel methods modified with ionic liquid and surfactant molecules, Chem. Mater. 18 (2015) 5377-5384.

[16] F.T. Li, Q. Wang, X.J. Wang, B. Li, Y.J. Hao, R.H. Liu, D.S. Zhao, In-situ one-step synthesis of novel BiOCl/$Bi_{24}O_{31}Cl_{10}$ heterojunctions via self-combustion of ionic liquid with enhanced visible-light photocatalytic activities, Appl. Catal. B 150 (2014) 574-584.

[17] C.Y. Yang, F. Li, T.H. Li, A one-step ionic liquid-assisted ultrasonic method for the preparation of BiOCl/m-$BiVO_4$ heterojunctions with enhanced visible light photocatalytic activity, CrystEngComm 17 (2015) 7676-7683.

[18] J. Wang, Z. Jiang, Z.H. Zhang, Y.P. Xie, X.F. Wang, Z.Q. Xing, R. Xu, X.D. Zhang, Sonocatalytic degradation of acid red B and rhodamine B catalyzed by nano-sized ZnO powder under ultrasonic irradiation, Ultrason. Sonochem 15 (2008) 768-774.

[19] J. Wang, Z. Jiang, L.Q. Zhang, P.L. Kang, Y.P. Xie, Y.H. Lv, R. Xu, X.D. Zhang, Sonocatalytic degradation of some dyestuffs and comparison of catalytic activities of nano-sized TiO_2, nano-sized ZnO and composite TiO_2/ZnO powders under ultrasonic irradiation, Ultrason. Sonochem 16 (2009) 225-231.

[20] J. Wang, Z.J. Pan, Z.H. Zhang, X.D. Zhang, F.Y. Wen, T. Ma, Y.F. Jiang, L. Wang, L. Xu, P.L. Kang, Sonocatalytic degradation of methyl parathion in the presence of nanometer and ordinary anatase titanium dioxide catalysts and comparison of their sonocatalytic abilities, Ultrason. Sonochem 13 (2006) 493-500.

[21] J. Wang, Y.H. Lv, L.Q. Zhang, B. Liu, R.Z. Jiang, G.X. Han, R. Xu, X.D. Zhang, Sonocatalytic degradation of organic dyes and comparison of catalytic activities of CeO_2/TiO_2, SnO_2/TiO_2 and ZrO_2/TiO_2 composites under ultrasonic irradiation, Ultrason. Sonochem 17 (2010) 642-648.

[22] M.L. Guan, D.K. Ma, S.W. Hu, Y.J. Chen, S.M. Huang, From hollow olive-shaped $BiVO_4$ to n-p core-shell $BiVO_4$@Bi_2O_3 microspheres: Controlled synthesis and enhanced visible-light-responsive photocatalytic properties, Inorg. Chem. 50 (2010) 800-805.

[23] X.C. Zhang, X.X. Liu, C.M. Fan, Y.W. Wang, Y.F. Wang, Z.H. Liang, A novel BiOCl thin film prepared by electrochemical method and its application in photocatalysis. Appl. Catal. B 132 (2013) 332-341.

[24] S.W. Zhu, Q.G. Li, F. Li, W. Cao, T.H. Li, One-pot synthesis of Ag^+ doped $BiVO_4$ microspheres with enhanced photocatalytic activity via a facile hydrothermal method, J. Phys. Chem. Solids. 92 (2016) 11-18.

[25] Z.B. Xiang, Y. Wang, D. Zhang, P. Ju, BiOI/$BiVO_4$ p-n heterojunction with enhanced photocatalytic activity under visible-light irradiation, J. Ind. Eng. Chem. 40 (2016) 83-92.

[26] S.M. Thalluri, M. Hussain, G. Saracco, J. Barber, N. Russo, Green-synthesized $BiVO_4$ oriented along {040} facets for visible-light-driven ethylene degradation, Ind. Eng. Chem. Res. 53 (2014) 2640-2646.

[27] L.M. Hua, S.Y. Dong, Q.L. Li, J.L. Feng, Y.Q. Pi, M.L. Liu, J.Y. Sun, J.H. Sun, Facile synthesis of BiOF/Bi_2O_3/reduced graphene oxide photocatalyst with highly efficient and stable natural sunlight photocatalytic performance, J. Alloy. Compd. 633 (2015) 256-264.

[28] W. Att, M. Takeuchi, T. Suzuki, K. Kubo, M. Anpo, T. Ogawa, Enhanced osteoblast function on ultraviolet light-treated zirconia, Biomaterials 30 (2009) 1273-1280.

[29] G. Swain, S. Sultana, B. Naik, K. Parida, Coupling of crumpled-type novel MoS_2 with CeO_2 nanoparticles: a noble-metal-free p-n heterojunction composite for visible light photocatalytic H_2 production. ACS Omega. 2 (2017) 3745-3753.

[30] D. Kandi, S. Martha, A. Thirumurugan, K.M. Parida, CdS QDs-decorated self-doped γ-Bi_2MoO_6: a sustainable and versatile photocatalyst toward photoreduction of Cr (VI) and degradation of phenol, Acs Omega. 2 (2017) 9040-9056.

[31] D. Kandi, S. Martha, A. Thirumurugan, K.M. Parida, Modification of BiOI microplates with CdS QDs for enhancing stability, optical property, electronic behavior toward rhodamine B decolorization, and photocatalytic hydrogen evolution, J. Phys. Chem. C. 121 (2017) 4834-4849.

[32] D. Kandi, D.P. Sahoo, S. Martha, K.M. Parida, Rational design of a coupled confronting Z-Scheme system toward photocatalytic refractory pollutant degradation and water splitting reaction, Adv. Mater. Interfaces 6 (2019) 1900370.

[33] A. Behera, D. Kandi, S. Martha, K.M. Parida, Constructive interfacial charge carrier separation of a p-$CaFe_2O_4$@n-$ZnFe_2O_4$ heterojunction architect photocatalyst toward photodegradation of antibiotics, Inorg. Chem. 58 (2019) 16592-16608.

[34] B.C. Hodges, E.L. Cates, J.H. Kim, Challenges and prospects of advanced oxidation water treatment processes using catalytic nanomaterials, Nature Nanotech 13 (2018) 642-650.

Figure captions

Fig. 1 XRD patterns of the samples prepared at different pH values.

Fig. 2 The high magnification SEM image of the samples synthesized at different pH values: (a) BiF_3 (S1), (b) BiOF/Bi_2O_3 (S2), (c) BiOF/Bi_2O_3 (S3), (d) BiOF/Bi_2O_3 (S4), (e) BiOF/BiF_3 (S5), (f) BiOF/BiF_3 (S6), (g) BiOF/Bi_2O_3 (S7), (h) BiOF/Bi_2O_3 (S9), (i) BiOF/Bi_2O_3 (S11).

Fig. 3 TEM and HRTEM images of the BiOF/Bi_2O_3 (S2).

Fig. 4 The XPS spectra of S2: (a) survey spectrum, XPS high-resolution spectrum of (b) Bi 4f, (c) O 1s, (d) F 1s.

Fig. 5 UV-vis diffuse reflectance spectra of BiOF/Bi_2O_3 samples prepared at (a) pH = 2, 3, 4, (b) pH = 7, 9, 11. PL spectra of BiOF/Bi_2O_3 samples prepared at (c) pH = 2, 3, 4, (d) pH = 7, 9, 11.

Fig. 6 Time-course variation of C/C_0 of RhB under UV light illumination over BiOF/Bi_2O_3 prepared at (a) pH = 2, 3, 4, (b) pH = 7, 9, 11.

Fig. 7 Time-course variation of C/C_0 of RhB under (a) visible light irradiation + three drops of H_2O_2, (b) visible light irradiation over BiOF/Bi_2O_3 prepared at different pH values.

Fig. 8 Time-course variation of C/C_0 of RhB under (a) ultrasonic irradiation + three drops of H_2O_2, (b) ultrasonic irradiation over BiOF/Bi_2O_3 prepared at different pH values.

Fig. 9 Time course of the (a) photodegradation (b) sonodegradation of RhB over the as-synthesized BiOF/Bi_2O_3 (S2) in the presence of different radicals scavengers, (c) fluorescence spectra of S2 in basic solution of terphthalic acid.

Scheme 1 The proposed mechanism for (a) photocatalysis (b) sonocatalysis of the BiOF/Bi_2O_3 catalyst.

Figures

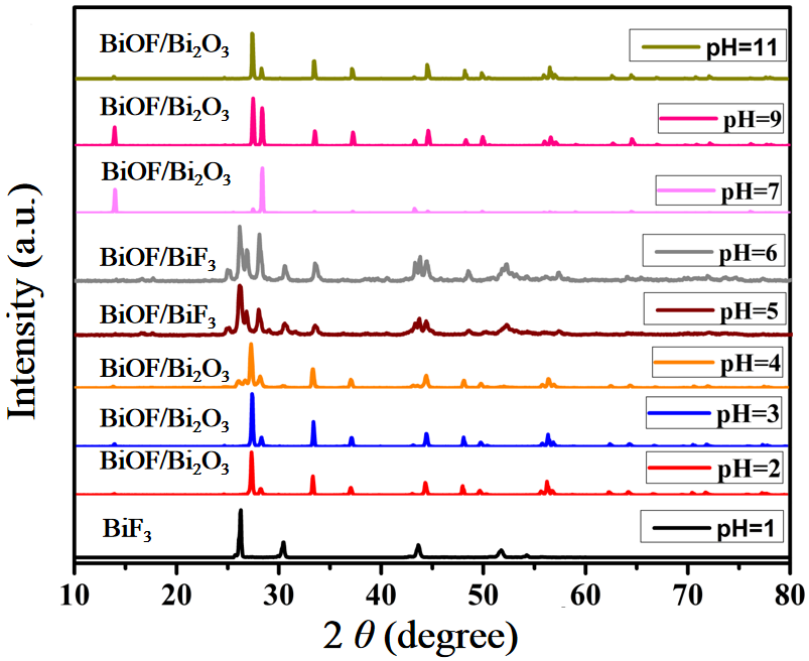

Fig. 1

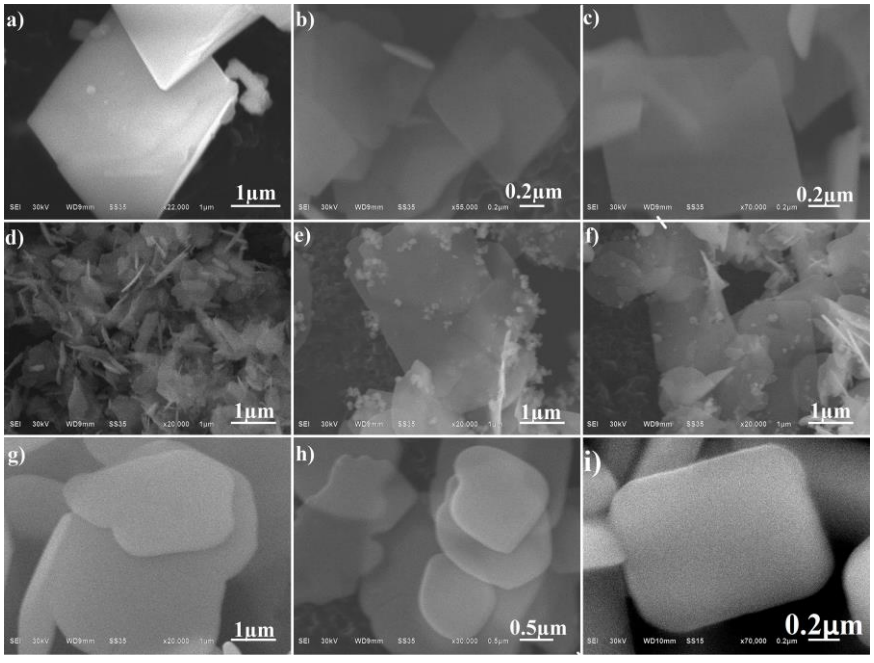

Fig. 2

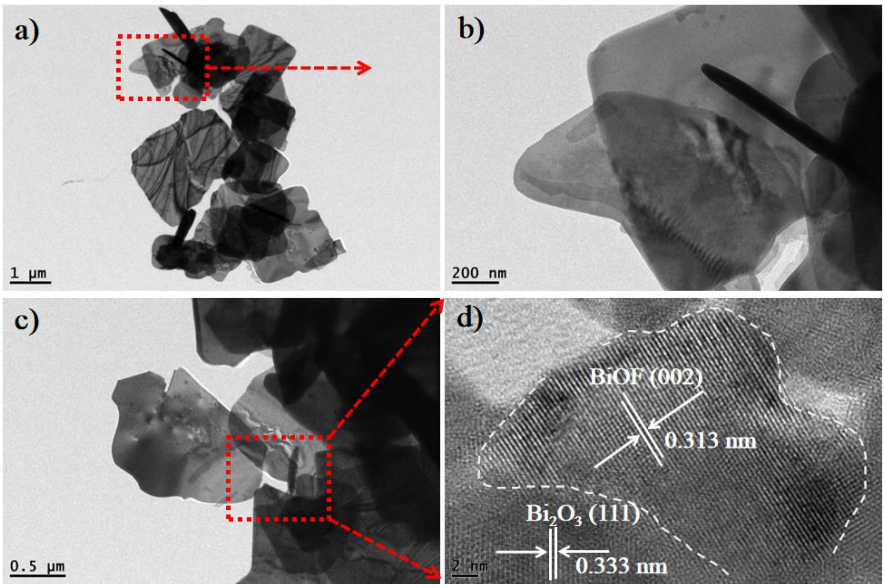
a)
1 μm
b)
200 nm
c)
0.5 μm
d)
BiOF (002)
0.313 nm
Bi2O3 (111)
0.333 nm
2 nm

Fig. 3

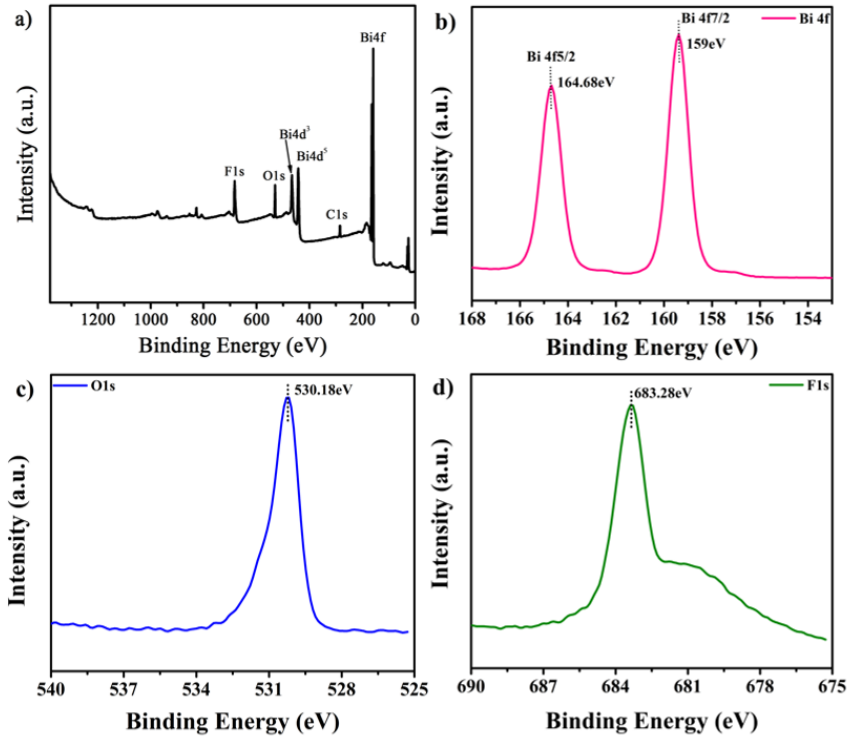
a)
Bi4f
Bi4d3
Bi4d5
F1s
O1s
C1s
Intensity (a.u.)
1200 1000 800 600 400 200 0
Binding Energy (eV)
b)
Bi 4f7/2
Bi 4f
Bi 4f5/2
164.68eV
159eV
Intensity (a.u.)
168 166 164 162 160 158 156 154
Binding Energy (eV)
c)
O1s
530.18eV
Intensity (a.u.)
540 537 534 531 528 525
Binding Energy (eV)
d)
683.28eV
F1s
Intensity (a.u.)
690 687 684 681 678 675
Binding Energy (eV)

Fig. 4

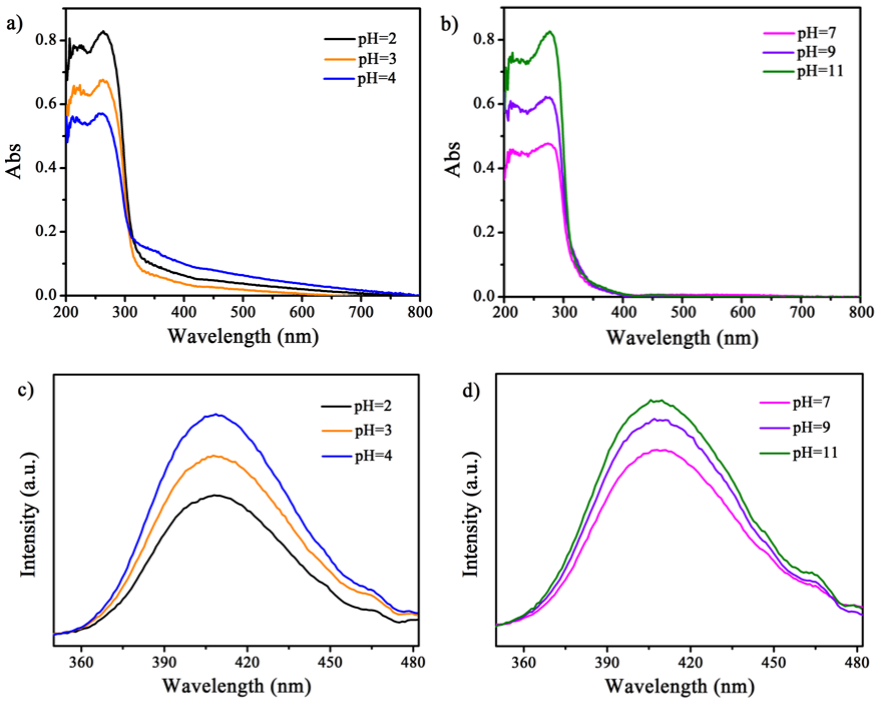
a)
Abs
Wavelength (nm)
pH=2
pH=3
pH=4
b)
Abs
Wavelength (nm)
pH=7
pH=9
pH=11
c)
Intensity (a.u.)
Wavelength (nm)
pH=2
pH=3
pH=4
d)
Intensity (a.u.)
Wavelength (nm)
pH=7
pH=9
pH=11

Fig. 5

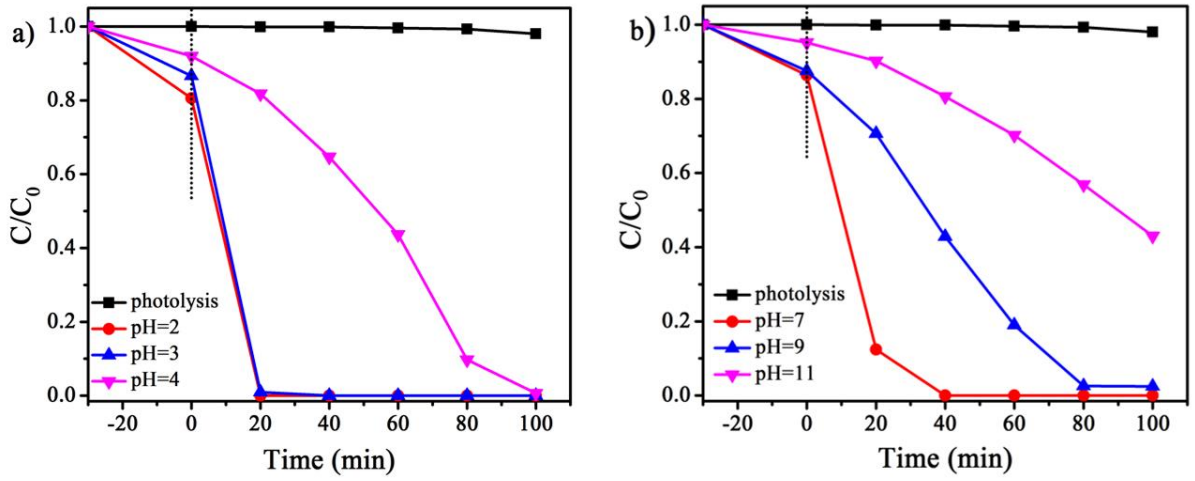
a)
C/C0
Time (min)
photolysis
pH=2
pH=3
pH=4
b)
C/C0
Time (min)
photolysis
pH=7
pH=9
pH=11

Fig. 6

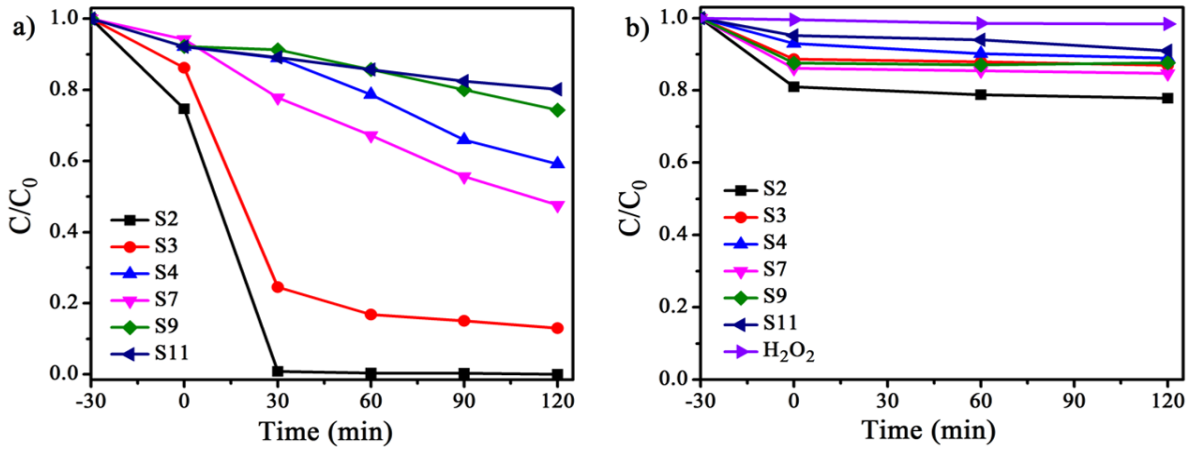
a)
b)
C/C0
Time (min)
S2
S3
S4
S7
S9
S11
H2O2

Fig. 7

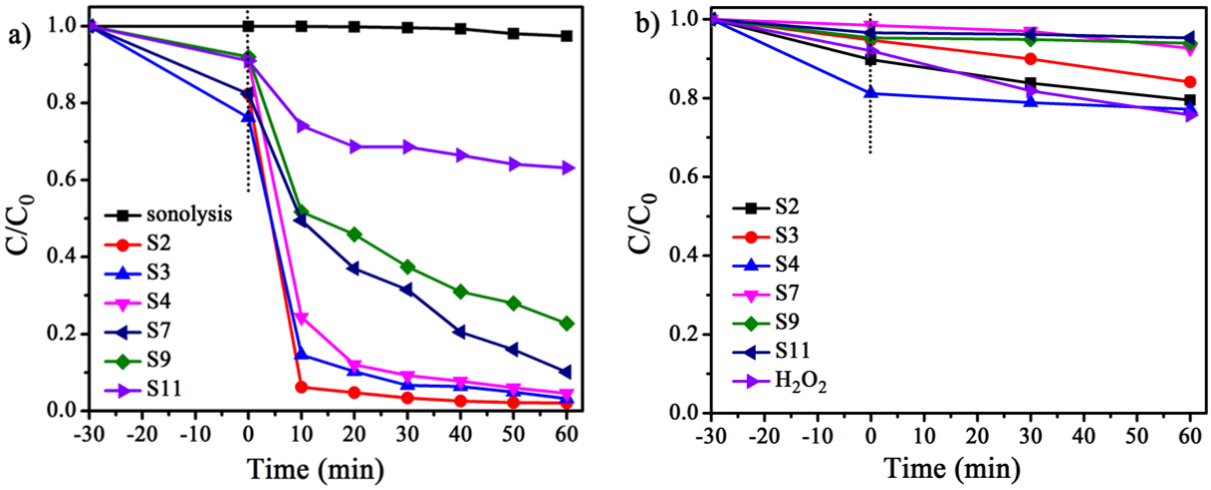
a)
b)
C/C0
Time (min)
sonolysis
S2
S3
S4
S7
S9
S11
H2O2

Fig. 8

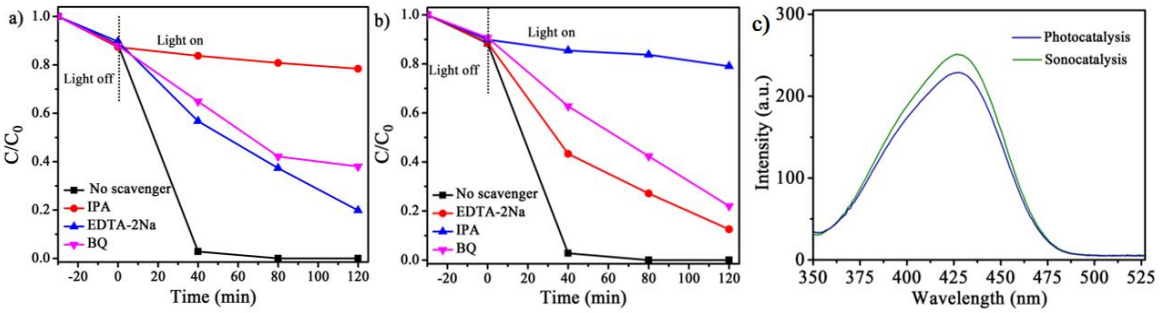

Fig. 9

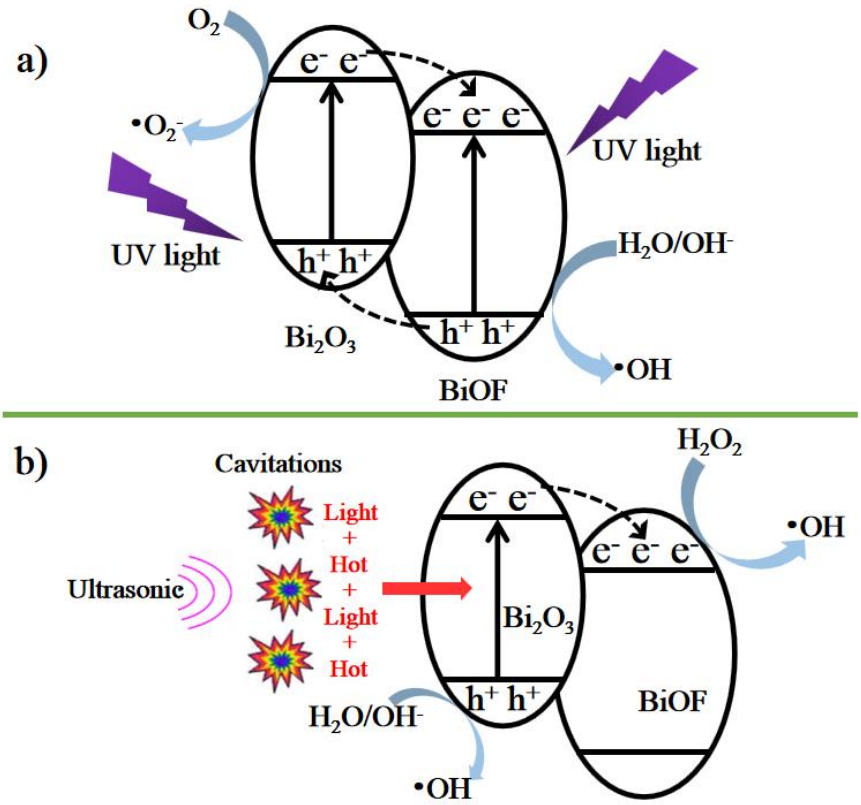

Scheme 1